

1

2 **Title**

3 Flow cytometry method for absolute counting and single-cell phenotyping of  
4 mycobacteria

5

6 **Authors**

7 David A. Barr \*,<sup>1,3,4</sup> Charles Omollo,<sup>2</sup> Mandy Mason,<sup>2</sup> Anastasia Koch,<sup>2</sup> Robert J.  
8 Wilkinson,<sup>1,5,6,7</sup> David G. Lalloo,<sup>4</sup> Graeme Meintjes,<sup>1,5</sup> Valerie Mizrahi,<sup>2,1</sup> Digby F.  
9 Warner,<sup>2,1</sup> Gerry Davies.<sup>3</sup>

10 \* Corresponding author

11 [david.barr@liverpool.ac.uk](mailto:david.barr@liverpool.ac.uk)

12

13 **Affiliations:**

- 14 1. Wellcome Centre for Infectious Diseases Research in Africa (CIDRI-Africa),  
15 Institute of Infectious Disease and Molecular Medicine, University of Cape  
16 Town, Observatory 7925, Cape Town, South Africa.
- 17 2. SAMRC/NHLS/UCT Molecular Mycobacteriology Research Unit, DST/NRF  
18 Centre of Excellence for Biomedical TB Research, Institute of Infectious  
19 Disease and Molecular Medicine, Division of Medical Microbiology,  
20 Department of Pathology, University of Cape Town, Cape Town, South  
21 Africa
- 22 3. Institute of Infection and Global Health, University of Liverpool, Liverpool  
23 L7 3EA, UK.
- 24 4. Liverpool School of Tropical Medicine, Pembroke Place, Liverpool L3 5QA,  
25 UK.
- 26 5. Department of Medicine, University of Cape Town, Cape Town, South  
27 Africa.
- 28 6. The Francis Crick Institute, London NW11AT, UK.
- 29 7. Department of Medicine, Imperial College, London, W12 0NN, United  
30 Kingdom.

31

32

## 33 Abstract

34 Detection and accurate quantitation of viable *Mycobacterium tuberculosis* is  
35 fundamental to understanding mycobacterial pathogenicity, tuberculosis (TB) disease  
36 progression and outcomes; TB transmission; drug action, efficacy and drug resistance.  
37 Despite this importance, methods for determining numbers of viable bacilli are  
38 limited in accuracy and precision owing to inherent characteristics of mycobacterial  
39 cell biology – including the tendency to clump, and “differential” culturability – and  
40 technical challenges consequent on handling an infectious pathogen under biosafe  
41 conditions. We developed an absolute counting method for mycobacteria in liquid  
42 cultures using a bench-top flow cytometer, and the low-cost fluorescent dyes Calcein-  
43 AM (CA) and SYBR-gold (SG). During exponential growth CA+ cell counts are  
44 highly correlated with CFU counts and can be used as a real-time alternative to  
45 simplify the accurate standardisation of inocula for experiments. In contrast to CFU  
46 counting, this method can detect and enumerate cell aggregates in samples, which we  
47 show are a potential source of variance and bias when using established methods. We  
48 show that CFUs comprise a sub-population of intact, metabolically active  
49 mycobacterial cells in liquid cultures, with CFU-proportion varying by growth  
50 conditions. A pharmacodynamic application of the flow cytometry method, exploring  
51 kinetics of fluorescent probe defined subpopulations compared to CFU is  
52 demonstrated. Flow cytometry derived *Mycobacterium bovis* BCG time-kill curves  
53 differ for rifampicin and kanamycin versus isoniazid and ethambutol, as do the  
54 relative dynamics of discrete morphologically-distinct subpopulations of bacilli  
55 revealed by this high-throughput single-cell technique.

## 56 Introduction

57 For more than 100 years, counting Colony Forming Units (CFU) has been the gold-  
58 standard for quantifying viable *Mycobacterium tuberculosis* (*Mtb*) bacilli, both *in*  
59 *vitro* and *ex vivo*. However, despite being a methodological foundation underpinning  
60 our scientific knowledge of *Mtb*, CFU counting has several technical and practical  
61 limitations, including cost and biosafety implications of maintaining multiple  
62 secondary cultures, time interval to results, loss of results from contamination, the  
63 inability to distinguish single cells from cell aggregates (clumps), and high intra- and  
64 inter-laboratory variation.<sup>1-3</sup>

65 More fundamentally, under some conditions sub-populations of viable *Mtb* cells do  
66 not form colonies and are therefore unobserved by CFU counting.<sup>4-6</sup> This is of  
67 particular relevance to tuberculosis (TB) diagnostics and research because of the  
68 prevailing theory that the existence of phenotypically heterogenous sub-populations  
69 of bacilli – with differential metabolic or growth states – underlie profound aspects of  
70 TB disease biology, such as latency and the need for prolonged therapy to effect  
71 sterilising cure.<sup>7-10</sup>

72 Improved methods for absolute counting of mycobacteria and phenotypic  
73 characterisation of subpopulations are therefore desirable. Flow cytometry (FCM)  
74 is a well-established technique for counting and characterising eukaryotic  
75 cells, and its potential to advance single-cell analyses in microbiology has been  
76 discussed in depth.<sup>11,12</sup> Several groups have applied FCM to mycobacteria, including  
77 drug sensitivity testing,<sup>13-22</sup> investigation of cell biology,<sup>23-28</sup> early phase diagnostic  
78 test development,<sup>29,30</sup> live/dead discrimination,<sup>31,32</sup> and more advanced single-cell  
79 phenotyping.<sup>23,33,34</sup> Fluorescent dyes used by prior investigators include: probes of  
80 membrane integrity (the nucleic acid stains SYTOX-green,<sup>33</sup> SYTO-9,<sup>24,31,32</sup> SYTO-  
81 BC,<sup>24,32</sup> SYTO-16,<sup>16,28</sup> SYBR-green I,<sup>30</sup> propidium iodide,<sup>16,24,31,32,35</sup> TO-PRO-3  
82 iodide,<sup>34</sup> and auramine-O<sup>13,35,36</sup>); probes of metabolic activity (esterase substrate dyes  
83 fluorescein diacetate,<sup>14,17,20,21,37</sup> and Calcein-violet<sup>33</sup>) and membrane potential  
84 (diethyloxycarbocyanine iodide<sup>25,34</sup> & rhodamine-123<sup>27</sup>). In general, absolute bacillary  
85 counts have not been derived from FCM; instead, batch measures of fluorescence  
86 (*e.g.* mean fluorescence signal),<sup>13-17,20,21,27,29,37</sup> qualitative read-outs (*e.g.* scatter-  
87 plots),<sup>18,26,34</sup> or percentages<sup>23,25,33</sup> are reported. Growth conditions, processing (*e.g.*

88 washes and fixation), and staining protocols vary widely. In the few cases in which  
89 the same stains have been used by different groups, results are often contradictory: for  
90 example, propidium iodide is reported to stain 0% of heat killed *M. tuberculosis* by  
91 one study,<sup>38</sup> and 100% by another.<sup>31</sup> No comparisons of FCM counts with CFU  
92 enumerations have been published.

93 The aims of the current study were:

- 94 1) To develop and validate a method for absolute counting of mycobacteria *in vitro*  
95 using FCM.
- 96 2) To explore the use of fluorescent dyes as probes of cell function to define  
97 subpopulations of bacilli in discrete physiological states.
- 98 3) To compare dynamics of FCM-defined subpopulations and CFU in liquid cultures  
99 over time (growth curves), and over time in the presence of antimycobacterial  
100 compounds (time-kill curves).

101 We report a method developed on a low-cost flow cytometer (BD Accuri<sup>TM</sup> C6),  
102 using two commercially available fluorescent dyes (SYBR®-Gold and Calcein-AM).  
103 The BD Accuri C6 flow cytometer has fixed alignment and pre-optimised detector  
104 settings, can record volume of sample processed without use of counting beads, and is  
105 small enough to fit on a benchtop or inside a bio-containment hood. SYBR®-Gold  
106 (SG), a proprietary cyanine dye (excitation ~495nm, emission ~573nm) with >1000-  
107 fold fluorescence enhancement when bound to nucleic acid, was designed for use in  
108 gel electrophoresis.<sup>39</sup> SG has previously been shown to have substantially greater  
109 sensitivity than auramine-O for quantitative fluorescence microscopy of heat-fixed  
110 mycobacteria (99% versus 65-80%),<sup>40</sup> but it has not been applied in FCM. Calcein-  
111 AM (CA) is a non-polar, lipophilic ester which becomes charged and fluorescent  
112 when hydrolysed by ‘house-keeping’ esterases ubiquitous in the cytoplasm of living  
113 cells.<sup>41</sup> Hendon-Dunn and colleagues previously showed that the fluorescence of  
114 mycobacteria stained with Calcein-violet-AM correlated with rate of growth in a  
115 chemostat and declined with antimicrobial killing of bacilli.<sup>33</sup>

116 In the present study, we applied SG staining after heat killing bacilli to define a total  
117 intact cell count denominator; SG staining without heat killing to probe cell  
118 membrane integrity as a marker of death or damage; and CA staining without heat  
119 killing to probe metabolic activity as a marker of vitality.

120

## 121 Results

### 122 **Setting fluorescence threshold values for FCM events improves validity** 123 **of absolute bacilli counts**

124 The BD Accuri C6 flow cytometer has a fixed dynamic range for voltage and gain,  
125 but allows thresholds to be set on two signal values from light scatter and/or  
126 fluorescence channels. Signals below the set threshold are not recorded as events. For  
127 absolute counting of cells, an optimal threshold is one that is not so high as to exclude  
128 true events (signals from cells), yet high enough that it excludes electronic noise and  
129 signal from debris (which can otherwise mask true events owing to the refractory  
130 period of photodetectors). Typically, thresholds are set on forward and/or side scatter  
131 of light (FSC and SSC), as this allows fluorescence-positive and -negative events to  
132 be recorded without biasing measurements from the fluorescence channels.

133 We investigated different threshold strategies as follows. Mid-log phase *M. bovis*  
134 BCG cultures were analysed after 2-fold dilution in 0.15% v/v Tween80 PBS  
135 solution. These were compared to an identical preparation of cell-free 7H9 broth as a  
136 negative control. Permutations of threshold settings were screened. In each case a gate  
137 was set around an apparent discrete population of events visible on a log(SSC) by  
138 log(FSC) plot, with the gate set manually to minimise the ratio between negative  
139 control and the paired BCG sample event counts. The optimal ratio (false positive  
140 event count in cell free broth divided by the paired BCG culture count) was defined as  
141 the false discovery rate; therefore, threshold parameters which maximised the  
142 absolute count in the BCG broth gate and minimised the false discovery rate were  
143 sought.

144 Optimal threshold values based on light scatter (FSC and SSC) were inconsistent  
145 across replicates and were never associated with false discovery rates less than 10%.  
146 By contrast, thresholding on SSC and fluorescence (FL1 533/30 nm) in heat-killed,  
147 SYBR-gold stained mid-log BCG consistently reduced the false discovery rate to  
148 <0.5%, at the same time increasing absolute cell counts by more than one logarithm  
149 compared with thresholding on light scatter alone on the same samples (figure 1).  
150 Further, this strategy reduced the coefficient of variation between technical replicates

151 to <5%, and gave near perfect linearity across serial dilutions of the same sample  
152 ( $R^2 > 0.99$ ) (figure 1).

### 153 **Clumping in mycobacterial broth cultures can be observed and** 154 **quantified using FCM**

155 In all mycobacterial broth cultures tested – *M. bovis* BCG, *M. tuberculosis*, and *M.*  
156 *smegmatis*, a second population of events with higher FSC and SSC became evident  
157 from early log-phase onwards, developing into the dominant population in mid- or  
158 late log-phase (figure 2A). To investigate the nature of these distinct populations,  
159 events gated on the two light-scatter populations were sorted for downstream  
160 microscopy (figure 2 B&C). This analysis revealed that the higher light-scatter  
161 population was composed of clumped cells, despite the fact that all cultures were  
162 grown in detergent (Tween80, 0.1% to 0.25% v/v) under continuous agitation (150 to  
163 200 rpm), and notwithstanding the use of sonication prior to flow cytometry.

### 164 **Clumping is a major determinant of CFU count & can be controlled by** 165 **needle emulsification, but not vortex, sonication or centrifugation**

166 Having established the ability to quantify mycobacterial clumping in broth cultures  
167 using FCM, we next tested the comparative efficacies of standard microbiological  
168 methods for clump dispersal. Vortex and sonication failed to disrupt the clumped  
169 population observed on FCM; by contrast, needle emulsification of the broth culture  
170 largely eliminated clumping (figure 3A). Disruption of clumps by needle  
171 emulsification increased the single-cell population seen on FCM, and therefore the  
172 CFU count, by more than 0.5 log (figure 3B). Larger clumps not disrupted even by  
173 needle-emulsification emerged in late-stage broth cultures (figure 4).

174 A standard method for preparation of single-cell suspensions of mycobacteria is  
175 centrifugation, based on the premise that cell clumps are selectively pelleted by  
176 gravity, with single cells remaining in suspension.<sup>42</sup> However, using FCM we found  
177 that the ratio of clumps to single-cells was unaffected by centrifugation (figure 5).

### 178 **Growth dynamics of FCM-defined bacilli populations compared to CFU**

179 A FCM protocol for absolute counting of bacilli – incorporating SYBR-gold or  
180 Calcein-AM staining, needle-emulsification to disperse clumps, and thresholding on

181 fluorescence (summarised in figure 6) – was used to explore dynamics of *M. bovis*  
182 BCG growth in broth culture. We defined three FCM populations using this protocol:

183 1. **Calcein-AM-positive (CA+)** – live sample stained with Calcein-AM, to give  
184 an esterase positive, or ‘metabolically active’, cell count.

185 2. **SYBR-gold-positive (SG+)** – live sample stained with SYBR-gold, to count  
186 cells which have membranes permeable to SYBR-gold, implying membrane  
187 damage.

188 3. **Heat-killed ‘total cell count’ (HK)** – sample incubated in water-bath at 60°C  
189 for 12 minutes to permeabilise cell-membranes, followed by SYBR-gold  
190 staining. This is proposed to give a total count of intact cells containing  
191 nucleic acid, and therefore provides a denominator for calculating the  
192 proportion of cells which are CA+, or SG+, or colony-forming. The selected  
193 heat-kill time and temperature were selected as the minimum to reliably  
194 maximise the HK count.

195 CFU counts after needle emulsification were determined in parallel (figure 6).

196 In all culture growth phases (lag, log, stationary), the HK cell count was greater than  
197 CA+, SG+, or CFU counts (figure 7A), and was accepted as a total cell count. During  
198 log-phase, most cells were CA+ and colony forming, with SG+ cells constituting a  
199 minority sub-population (figure 7B-D). When entering stationary phase, CA+ and  
200 CFU counts started to fall, with a simultaneous rise in SG+ cells, which subsequently  
201 became the dominant subpopulation (figure 7B-D).

202 Correlation between CFU and CA+ counts was growth-phase dependent (figure 7E)  
203 with close co-variance in early-to-mid-log phase progressively diminishing in late-log  
204 (when CFU > CA+) and stationary phase (when CA+ > CFU). Total population  
205 growth rate – defined using the instantaneous rate-of-change of the log HK total cell  
206 count (the slope of the tangent to the curve at a given timepoint, *i.e.* the first-  
207 derivative) – correlated with the proportion of bacilli which were CA+, but not the  
208 proportion of bacilli forming colonies (figure 7F).

209 ***In vitro* pharmacodynamics of *M. bovis* BCG by CFU and FCM counting**

210 Having established growth dynamics in the absence of antimicrobials, the FCM count  
211 method was applied to pharmacodynamic (PD) time-kill analysis of *M. bovis* BCG.  
212 Starter cultures (100 ml in 500ml tissue culture flasks containing 0.15% v/v Tween 80  
213 7H9 medium) were grown to a density of  $\sim 2 \times 10^5$  CA+ cells per ml, then split into  
214 20ml samples in 50ml conical flasks. Antimicrobials (rifampicin, isoniazid,  
215 kanamycin, ethambutol) were added at a range of final concentrations in multiples of  
216 their minimum inhibitory concentration (MIC99), and bacilli quantified at 0, 24, 48,  
217 72 and 120 hours using FCM and CFU counting. The experiment was repeated on  
218 three separate occasions to ensure independent biological replicates.

219 Raw FCM data plots for heat-killed, Calcein-AM, and SYBR-gold stained  
220 preparations from one of three independent replicates are shown for selected  
221 conditions in figure 8A-C. Time-kill curves based on absolute counts, and proportions  
222 (CA+/HK, SG+/HK, CFU/HK counts), are shown in figures 9A & 9B, respectively.

223 Compared to antimicrobial-free controls, total cell count (HK count) growth was  
224 generally impeded by the presence of antimicrobials, although exponential growth  
225 still occurred with ethambutol and kanamycin at 0.5xMIC concentration of both  
226 antimicrobials. Critically, even at high concentrations of all antimicrobials tested, HK  
227 count did not show dramatic reduction over 120 hours of exposure.

228 By contrast, CA+ and CFU counts fell substantially over that time period. Notably,  
229 CFU counts declined earlier than CA+ counts for all antimicrobial tested for all  
230 inhibitory concentrations. Rifampicin or kanamycin exposure resulted in an earlier  
231 decline in CA+ counts than was observed for isoniazid or ethambutol, which at high  
232 concentrations showed an initial increase in proportion of cells CA+ at 24 hours,  
233 before a sustained fall to day 5.

234 Because a fraction of cells were SG+ under any condition, the major driver of  
235 absolute SG+ count was the total cell count, this can be seen in the antimicrobial-free  
236 controls where the highest SG+ counts were seen at late stages of growth. The  
237 proportion SG+ was, however, antimicrobial dependent: SG+ cells were a majority by  
238 day 5 in all supra-MIC concentration conditions, but the rise in the SG+ proportion  
239 occurred earlier and was larger for isoniazid and ethambutol than for rifampicin or  
240 kanamycin.



241 To summarise differing effects by antimicrobial and subpopulation, sigmoidal  $E_{\max}$   
242 models were fitted to the time-kill data (figure 10). Based on CFU time-kill curves,  
243 rifampicin, kanamycin, and isoniazid all have similar  $E_{\max}$  values, while ethambutol is  
244 substantially lower. CA+ time-kill  $E_{\max}$  was higher for rifampicin and kanamycin; and  
245 lower for ethambutol and isoniazid. The pattern was reversed for the effect on SG+  
246 proportion. Finally, while the effects of antimicrobials on total cell count (HK count)  
247 were modest, they did differ by antimicrobial, with  $E_{\max}$  highest for rifampicin and  
248 lowest for ethambutol.

### 249 **Subpopulations of cells by SYBR-gold staining characteristics**

250 In addition to count data, qualitative differences in fluorescence were seen in live  
251 bacilli stained with SYBR-gold, with two subpopulations of SG+ cells separated by  
252 FL1 intensity (most distinct after 72 hours of isoniazid or ethambutol exposure, figure  
253 8C). We hypothesised that two populations of bacilli with different SG staining  
254 properties were revealed by the membrane permeabilising effects of these  
255 antimicrobials. To investigate this possibility, we developed a protocol for  
256 permeabilising *M. bovis* BCG membranes without bacillary destruction (detailed in  
257 methods), and characterised these subpopulations under different antimicrobial  
258 conditions by quantifying them and through direct microscopy after cell-sorting.

259 Dual SG+ subpopulations were discriminated by distribution peaks (figure 11A) and  
260 were seen under all conditions, including growth without antimicrobial exposure  
261 (figure 11B) with one population (labelled P2) returning a mean fluorescence two-  
262 fold higher than the other (labelled P1) (figure 11A&C). Fluorescent microscopy of  
263 cell-sorted samples showed that, compared to P1, P2 bacilli were longer (mean 4.0 $\mu$ m  
264 versus 2.5 $\mu$ m), with double the number of fluorescent foci (mean 6.1 versus 3.2)  
265 (figure 11D). The ratio of P2 to P1 cells in antimicrobial-free cultures was median  
266 1.75, and non-significantly higher when bacilli were exposed to rifampicin or  
267 kanamycin (median 1.83 and 1.86, respectively), but significantly higher after  
268 exposure to ethambutol or isoniazid (median 2.11 and 2.00, respectively;  $p < 0.001$  for  
269 both by rank-sum test). The P2:P1 ratio when bacilli were incubated with both  
270 rifampicin and isoniazid matched rifampicin mono-exposure rather than isoniazid  
271 mono-exposure (figure 11E).

272

## 273 Discussion

274 Detection and accurate quantitation of *Mycobacterium tuberculosis* is fundamental to  
275 understanding TB biology. Growing evidence suggests that culture-based methods  
276 detect only a sub-population of bacilli,<sup>4,5</sup> yet these methods remain standard in  
277 mycobacterial sciences. By contrast, in response to the analogous problem of  
278 differential culturability of microbiota in environmental substrates, FCM has been  
279 adopted as an essential method in environmental microbiology research,<sup>60,61</sup> and  
280 industry.<sup>62,63</sup> We developed a novel FCM-based method for absolute counting of  
281 mycobacteria in liquid cultures. While several groups have reported characterising  
282 mycobacteria using FCM, our method is the first to give absolute counts, and can be  
283 used to quantify total cell denominator, the presence of cell-clumps, and sub-  
284 populations with metabolic activity (using the esterase substrate, Calcein-AM) or  
285 membrane permeability (using the nucleic acid stain, SYBR-gold). Our results  
286 highlight some critical shortcomings of current ‘gold-standard’ methods for  
287 mycobacteria quantification. We also illustrate how the FCM absolute count method  
288 can be used for high-throughput, rapid investigations of phenotypic heterogeneity in  
289 mycobacteria and demonstrate the capacity to extract pharmacodynamic data using  
290 this approach.

291 Using our FCM method we found that we could reliably identify a subpopulation of  
292 the batch culture comprising clumped cells. Further investigations revealed that  
293 mycobacterial cultures remain prone to cell clumping in spite of commonly used  
294 measures to reduce their formation and to disrupt these before experimentation. We  
295 found that sample processing has a major impact on clump-dispersal, such that needle  
296 emulsification could increase CFU count approximately two-fold even in early log-  
297 phase growth. This implies the potential for significant noise and bias in CFU  
298 determination, especially for late-log and stationary phase cultures, given that the  
299 method depends on serial dilution of dispersed cultures. Our data suggest published  
300 protocols<sup>42</sup> for producing single cell suspensions using centrifugation have no effect  
301 on the ratio of clumps to single cells. Using the needle-emulsification and FCM  
302 counting methods described would be expected to reduce experimental error in  
303 mycobacterial research where bacilli counts are needed to standardise starting  
304 conditions, or where the number of bacilli is the dependent variable of interest.

305 Further, under antimicrobial-free early-mid log-phase growth conditions, CA+  
306 bacillary counts correlate well with CFU counts and can be obtained within 90  
307 minutes using low-cost reagents indicating that the FCM counting method is a  
308 practicable alternative to current culture-based methods of estimating cell numbers.

309 Our FCM method is distinct from previously described mycobacterial FCM protocols  
310 primarily because a fluorescence threshold is used to determine when FCM events are  
311 recorded. This means that fluorescence-negative events (e.g. a Calcein negative cell)  
312 cannot be directly observed but permits accurate absolute counts to be reported for the  
313 first time in mycobacterial flow cytometry. Because an absolute cell count  
314 denominator can be established with SYBR-gold staining of heat-killed bacilli, the  
315 proportion of bacilli with a given characteristic can be ascertained. Importantly, a total  
316 cell denominator also allows the proportion of bacilli forming colonies to be  
317 measured, which was about 60% in mid-exponential phase of growth in liquid culture.

318 Our pharmacodynamic results build on previous mycobacterial flow cytometry work  
319 reported by Hendon-Dunn *et al.*<sup>33</sup> We replicate their finding that pharmacodynamic  
320 flow cytometry profiles based on fluorescent probes of cytoplasmic esterase  
321 metabolism and cell wall integrity are different for drugs with different mechanisms  
322 of action. We found that the cell wall acting drugs isoniazid and ethambutol were  
323 associated with a relatively rapid rise in SG+ cells, while the cytoplasmic targeting  
324 rifampicin and kanamycin showed relatively early decline in CA+ bacilli. However,  
325 Hendon-Dunn *et al.* observed only a moderate, concentration-independent effect of  
326 rifampicin on Calcein-violet positive bacilli over the first 4 days of exposure. By  
327 contrast we found that rifampicin had an early, concentration-dependent effect on  
328 CA+ cells, and this effect was substantially greater than for isoniazid. Hendon-Dunn  
329 *et al.* measured relative proportions of Calcein positive and negative cells in  
330 cytometry plots, while our method produces absolute cell counts. If antimicrobials  
331 have differential effects on the total cell count (which we observed), relative  
332 proportions could be unreliable readouts of drug effect (owing to a ‘denominator  
333 fallacy’). In addition, the manual gating strategy used by Hendon-Dunn *et al.* does not  
334 appear to capture the shift in mean Calcein fluorescence seen under early rifampicin  
335 action, whereas the unsupervised classification approach implemented in this method  
336 does.

337 Again, based on absolute counts, we were able to directly and quantitatively compare  
338 CFU and FCM sub-population pharmacodynamics. Under all antimicrobial conditions  
339 tested, elimination of colony forming bacilli occurred substantially earlier than the  
340 decline in CA+ bacilli or the rise in SG+ bacilli. This means that, at some time points  
341 a majority of bacilli are structurally intact with evidence of metabolic activity but do  
342 not form colonies. Further, we show that pharmacodynamic effect estimates based on  
343 FCM-defined subpopulations give different read-outs from those based on CFU  
344 counts: the rifampicin effect on CFU elimination is similar to isoniazid, but rifampicin  
345 elimination of CA+ bacilli is markedly greater; rifampicin also has a larger effect on  
346 total cell count than the other antimicrobials tested. Rather than simply being a rapid  
347 surrogate for CFU counts, the FCM method therefore provides information on  
348 antimycobacterial drug pharmacodynamics not captured by CFU counting, but it is  
349 unknown if this information is clinically meaningful. Terminally injured bacilli may  
350 simply retain metabolic activity with residual enzyme activity in a non-viable cell.  
351 Alternatively, as non-growing metabolically active (NGMA) cells can be capable of  
352 resuscitation,<sup>55</sup> this may represent an adaptive response to antimicrobial stress by  
353 reducing the physiological consequences of target inhibition.<sup>56</sup> FCM probes of  
354 metabolic and structural integrity would then be more meaningful measures of  
355 viability. The latter would be a simple explanation for the lack of correlation between  
356 culture-based surrogate endpoints (early bactericidal activity measured using CFU  
357 counting, 2-month culture conversion, modelling serial CFU counts or time-to-  
358 positivity in liquid culture) and probability of achieving sterilising cure in clinical  
359 tuberculosis pharmacodynamics<sup>43</sup> and warrants testing in clinical samples.

360 If NGMA bacilli are an adaptive response to antimicrobial exposure then the ability to  
361 characterise them using high-throughput methods is critical. By staining live but  
362 membrane-permeabilized bacilli with SYBR-gold, we observed two distinct bacilli  
363 sub-populations, separated by a two-fold difference in mean fluorescence. We found  
364 this phenotype-variation was specifically induced by exposure to isoniazid or  
365 ethambutol, but the isoniazid effect was inhibited by the presence of rifampicin.  
366 Importantly, the induction of this phenotype could be seen at antimicrobial-condition-  
367 timepoints where >99.9% of CFU were already eliminated (e.g. after 72 hours of  
368 isoniazid exposure at 4x MIC concentration). After cell-sorting, bacilli from the two-  
369 fold brighter subpopulation were found to be longer with double the number of

370 fluorescence foci. Given that SYBR-gold fluoresces when bound to nucleic acid, this  
371 implies a bacillary phenotype with double the nucleic acid content, and this  
372 phenotypic heterogeneity may therefore represent different numbers of chromosome  
373 copies. In a non-human primate model of tuberculosis, “chromosomal equivalents”  
374 remain abundant in granulomas that have been sterilised (rendered CFU-negative) by  
375 isoniazid therapy.<sup>64</sup> Peaks separated by a 2-fold difference in fluorescent intensity  
376 after staining with ethidium bromide or PicoGreen have been used extensively to  
377 define multiple chromosome numbers in *E. coli*.<sup>44-46</sup> Further, several groups have  
378 associated polyploidy in *E. coli* with elongated “filamentous” persister cells capable  
379 of accelerated antibiotic resistance evolution.<sup>46-48</sup> In the Wayne model of non-  
380 replicating persistence during hypoxia-induced stress, mycobacteria are found to be  
381 diploid.<sup>49</sup> In an *in vitro* foamy-macrophage model, intracellular *Mycobacterium avium*  
382 has been shown to enter a reversible dormancy state where the bacilli elongate but do  
383 not divide (implying they would not form colonies);<sup>57</sup> it is suspected that these  
384 elongated, metabolically-active but non-replicating mycobacteria may be polyploid.<sup>50</sup>  
385 We speculate that polyploid, metabolically-active but non-colony forming bacilli  
386 which are preferentially induced by isoniazid but not rifampicin may be of significant  
387 clinical interest. If they represent a drug-tolerant phenotype unobserved by CFU  
388 counting, this could explain the fact that, while isoniazid has the most potent early  
389 bactericidal activity (EBA, measured by CFU counting), only rifampicin-containing  
390 regimens can reliably effect sterilising cure after 6-months (“short-course”) therapy.  
391 That drug resistant mutants emerge from phenotypically drug tolerant cells has  
392 recently been described for clinical isolates of *Staphylococcus aureus*,<sup>58</sup> a similar  
393 mechanism might exist for mycobacteria. The spontaneous drug resistance mutation  
394 rates for *M. tuberculosis in vitro* range from  $10^{-7}$  to  $10^{-9}$  and it is somewhat unclear if  
395 estimated total mycobacteria numbers *in vivo* allow for development of multidrug  
396 resistance through the simple product of these probabilities<sup>59</sup> – particularly if drug  
397 resistance emerges *de novo* after EBA has eliminated most bacilli observable by  
398 culture. A population of bacilli, unobserved by CFU counting but capable of  
399 elongation and polyploidy, implies ongoing chromosome replication after  
400 antimicrobial exposure and a pool of drug-tolerant cells from which drug resistance  
401 could emerge.

402 We used batch cultures in this work which may have limitations. Unexplained  
403 variation in FCM sub-population proportions and growth rates between biological  
404 replicates, even under antimicrobial-free conditions were seen (e.g. figure 7 B&F).  
405 Steady-state cultures – such as the chemostat method used by Hendon-Dunn in their  
406 flow-cytometry study – are known to improve reproducibility compared to batch  
407 cultures in microbial proteomics and transcriptomics analyses,<sup>51,52</sup> and are likely to be  
408 a major advantage in pharmacodynamic studies. Indeed, cell populations in batch  
409 cultures can show complex, non-linear growth patterns in cell size and DNA content<sup>44</sup>  
410 (which are major read-outs from the current implementation of our FCM absolute  
411 count method). However these limitations of batch cultures, match those of currently  
412 implemented culture methods in research laboratories and are expected to add noise  
413 rather than bias to our results.

414 Overall, our results add to the evidence of limitations in established methods for  
415 enumeration of bacilli and support the utility of FCM as a high-throughput, single-  
416 cell, culture-independent quantitative tool for the study of mycobacteria in preclinical  
417 drug development and ultimately in clinical samples.

418

## 419 **Methods**

### 420 **Cytometry**

421 Flow cytometry was performed on a BD Accuri™ C6 with manufacturer standard  
422 fluorescence detector set-up (FL1, 533/30 nm; FL2, 585/40 nm; FL3, > 670 nm; FL4,  
423 675/25 nm) and data acquisition with BD Accuri™ C6 software including recording  
424 processed sample volume. Quality assurance was performed using fluorescent beads  
425 as per manufacturer protocol. Manual and extended cleaning cycles were performed at  
426 the beginning and end of each flow cytometry session with verification of low event  
427 rate in filtered PBS before each run. Cell-sorting experiments were performed on a  
428 Bio Rad S3 cell sorter or FACS Vantage with voltage and gain set to recreate BD  
429 Accuri C6 plots. All microscopy was performed on a Zeiss Axio Observer 7.

### 430 **Sample processing**

431 Needle emulsification was performed with 12 passes through a double luer-lock ended,  
432 25 Gauge, 4-inch, micro-emulsifying needle (CAD7974 Sigma Aldrich). Sonication  
433 of cultures prior to FCM to assess effect on clump dispersal was performed by  
434 submerging 1ml centrifuge tubes attached to a flotation device in a benchtop  
435 ultrasonication water-bath three times for 30 second duration (Ultrawave™ U300HD  
436 30 KHZ; Ultrawave, Cardiff, UK). Heat-kill of mycobacterial samples for “HK  
437 counts” was by immersion of aliquots in a waterbath at 60°C for 12 minutes. Removal  
438 of antimicrobials prior to CFU plating was by pelleting a 1000µL sample (diluted 2-  
439 fold from 500µL with PBS) at 18000g for 12 minutes, removing 900µL of  
440 supernatant, resuspending 100µL residual volume in 900µL of 0.22um filtered 0.15%  
441 v/v Tween 80 sterile PBS by pipetting, repeated twice (for 10x10 = 100-fold dilution).  
442 This will have diluted antimicrobial in solution (unbound) 200-fold prior to plating.

#### 443 **Culture conditions**

444 Liquid media was prepared from Middlebrook 7H9 media (211887 BD Diagnostics)  
445 and 0.22um filtered deionized water according to manufacturer instructions. This was  
446 supplemented with 10% v/v Middlebrook OADC (212240 BD Diagnostics), 0.2% v/v  
447 glycerol and 0.15% v/v Tween 80. All broth was autoclaved prior to supplementation,  
448 and 0.22um filtered prior to use. Liquid cultures were at 37°C in the dark with 150-  
449 200rpm agitation in 50ml sterile polyethylene conical flasks in an incubator with an  
450 orbital shaking system (model LM-570; MRC Laboratory Instruments Group,  
451 London, UK).

452 Middlebrook 7H10 (262710 BD Diagnostics) agar was prepared with 0.22um filtered  
453 deionized water according to manufacturer instructions, with v/v 0.5% glycerol added  
454 before autoclave sterilisation. When cooled to 45°C, v/v 10% ADC supplement was  
455 added and tri-segmented plates poured to depth 5mm. For CFU counting, 10-fold  
456 serial dilutions of samples were prepared in 96-well plates using 0.22um filtered  
457 0.15% v/v Tween 80 sterile PBS. Each segment of a plate was inoculated with 50uL  
458 of serial dilutions and spread using disposable, sterile loop spreaders. CFU counts  
459 were performed with 3-fold technical replicates and counts averaged. Colony counts  
460 between 1 and 100 per segment were accepted and, after adjustment for dilution,  
461 averages across dilutions were made where available. Counts were performed on 3  
462 occasions (14, 21, and 28 days) to allow colonies to be counted before overgrowth.



## 463 **Reagents**

464 Primary stock dilutions of antibiotic powders were made in 100% DMSO and frozen  
465 at -20°C protected from light. Fresh working dilutions were prepared in PBS prior to  
466 each experiment, 0.22µm filtered, and stored wrapped in tin foil at 2-5°C refrigeration.  
467 Final concentrations of antimicrobials used in *M. bovis* BCG time-kill experiments are  
468 reported in multiples of the MIC as indicated. The MIC were: rifampicin, 0.01µg/ml;  
469 isoniazid 0.125µg/ml; kanamycin 1.0µg/ml; ethambutol 1.0 µg/ml.

470 Calcein-AM 50µg vials (ThermoFisher, C3100MP) were reconstituted in 50µL of  
471 DMSO on the day of each experiment, further diluted to 200µL with PBS for  
472 “working stock”. For cell staining, 5µL of working stock was added per 100µL of  
473 sample, with pipette mixing, then incubated in the dark at room temperature for 45-60  
474 minutes before resuspension of bacilli with pipetting. SYBR-gold proprietary stock  
475 (ThermoFisher, S-11494) was diluted 1000-fold in PBS, aliquoted and frozen at -20°C  
476 until use. After thawing aliquot, a further 10-fold dilution (to 10<sup>-4</sup>) in PBS was  
477 performed, and 5µL of this working stock added per 100µL of sample to be stained,  
478 with pipette mixing, followed by incubation in dark at room temperature for 45-60  
479 minutes before resuspension of bacilli with pipetting.

## 480 **Permeabilization of live cells**

481 For the investigation of SG stained subpopulations, published methods for  
482 permeabilizing mycobacterial cell walls were reviewed; those with highest reported  
483 success and best description of validation<sup>53,54</sup> were taken forward for testing and  
484 adaptation. Permutations of paraformaldehyde / ammonium chloride fixation, ethanol,  
485 hydrochloric acid, detergents, and lysozyme were tested at different concentrations,  
486 incubation times, and temperatures also assessed iteratively. This led to a final method  
487 for reliable permeabilization of BCG bacilli without substantial cell loss, such that  
488 over 80% of bacilli could be SYBR-gold stained (compared to the heat-killed total  
489 cell count denominator gold standard). In the final method, a 500µL sample was  
490 diluted to 1ml with PBS v/v 0.15% Tween 80, without wash step or fixation. After  
491 needle emulsification, lysozyme was added to final conc 0.1mg/ml, and the sample  
492 incubated for 45 minutes at 37°C. 500µl triton-X-100 was then added to final  
493 concentration v/v 0.2%. This was pelleted (16000g, 5 min) and re-suspended in 500µl



494 PBS-tween; 40µl working stock SYBR-gold added and incubated at room  
495 temperature for 2-4 hours.

## 496 **Data analysis**

497 Raw flow-cytometry data was extracted from .fcs files exported from BD Accuri C6  
498 software using *flowCore* (v 2.0.1) Bioconductor package<sup>65</sup> and all analysis performed  
499 in Rstudio v1.1.463. Rather than using manually placed gates to classify events,  
500 unsupervised machine-learning classification algorithms were used. For main flow  
501 cytometry plots (figure 8) k-means clustering was applied to FL1 height, FL1 area,  
502 and Side-Scatter height observations from one replicate using *kmeans()* function in  
503 *stats* package<sup>66</sup> in R, and the clustering solution applied to all the data. Optimal  
504 number of clusters was determined empirically using *NbClust()* function from  
505 *NBClust* package<sup>67</sup> in R. To separate P2 and P1 events in permeabilized SG-stained  
506 live cells (figure 11), a Gaussian Mixture Model was fit to all the data with 2  
507 component distributions using *normalmixEM()* function in *mixture* package.<sup>68</sup> In all  
508 FCM scatter plots, log transformations to base e (natural logarithms) are presented  
509 unless otherwise indicated (plots with log transformations to base 2 are used in cases  
510 where a doubling of fluorescence is a specific feature of interest).

511 Time-kill curves were summarised in descriptive plots (figure 9) using non-parametric  
512 loess regression models. To extract summary measures of antimicrobial effect, the  
513 time-kill data was modelled using a linear mixed-effects model, with a fixed effect of  
514 intercept, and random slopes for antibiotic condition and replicate:

$$\log_{cellcount} \sim intercept + (timepoint | condition) + (timepoint | rep)$$

515 This captures the crossed experimental design where each replicate was assessed  
516 under each antimicrobial condition, and each replicate assessed under each condition.  
517 The antibiotic condition effect, defined as slope gradient for the time-kill curve, was  
518 then extracted, independent of replicate effect, from the model as a summary PD  
519 measure. Because the dependent variable is on a log scale this assumes a mono-  
520 exponential decline in cell populations under antimicrobial action. The dependent  
521 variables assessed were CFU count, CA+ count, HK count, and proportion SG+. The  
522 R package *lme4* was used for this modelling.<sup>69</sup>

523 Antimicrobial effects extracted from these models were related to drug concentration  
524 for each antimicrobial using a standard sigmoid  $E_{max}$  PK/PD model, of form:

$$E = \frac{E_{max} \cdot C^n}{EC_{50}^n + C^n}$$

525 Where  $E$  is the PD effect (the slope gradient estimates by mixed-effects modelling  
526 above),  $C$  is the drug concentration (known from experimental condition), and the  
527 remaining parameters are estimated from the data:  $E_{max}$  (maximum achievable effect  
528 of antimicrobial),  $EC_{50}$  (the drug concentration where half of  $E_{max}$  is obtained), and  $n$   
529 (a scaling parameter). Models were fitted using non-linear least squares (nls()) function  
530 in R.

531 Fluorescence profiles of bacilli (figure 11D) were extracted as .csv files from  
532 microscopy images using Fiji (ImageJ).<sup>70</sup> This raw data was processed using a  
533 custom-built function defining local maxima in smoothed profiles to count fluorescent  
534 peaks.

535

536 **Acknowledgments:**

537 The work was supported by Wellcome Trust fellowship 105165/Z/14/A.

538 RJW receives support from Francis Crick Institute which is funded by Wellcome Trust  
539 [FL0010218], UKRI [FC0010218], CRUK [FC0010218] and also support from Wellcome  
540 Trust [104803, 203135].

541 **Author contributions:**

542 DAB, GD, DL, RJW, and GM conceived of the approach and initiated the project. DAB,  
543 DFW, VM, GD and GM conceived specific methods and experiments. DAB, CO, AK, and  
544 MKM designed and performed the experiments. DAB analysed data and wrote the manuscript  
545 with input from all authors.

546 **Data availability:**

547 Data and analysis scripts are available in an Open Science Framework repository here  
548 [https://osf.io/gwhpd/?view\\_only=02a61e8134cc4adca3840df604e0e38b](https://osf.io/gwhpd/?view_only=02a61e8134cc4adca3840df604e0e38b)

549 **Competing interests:**

550 Authors declare no competing interests

## References

1. Sutton S. Accuracy of plate counting. *Journal of Validation Technology* 2011; (Summer 2011): 42-6.
2. Hafner R, Cohn JA, Wright DJ, et al. Early bactericidal activity of isoniazid in pulmonary tuberculosis. Optimization of methodology. The DATRI 008 Study Group. *Am J Respir Crit Care Med* 1997; **156**(3 Pt 1): 918-23.
3. Sirgel F, Venter A, Mitchison D. Sources of variation in studies of the early bactericidal activity of antituberculosis drugs. *J Antimicrob Chemother* 2001; **47**(2): 177-82.
4. Chengalroyen MD, Beukes GM, Gordhan BG, et al. Detection and Quantification of Differentially Culturible Tubercle Bacteria in Sputum from Patients with Tuberculosis. *Am J Respir Crit Care Med* 2016; **194**(12): 1532-40.
5. Mukamolova GV, Turapov O, Malkin J, Woltmann G, Barer MR. Resuscitation-promoting factors reveal an occult population of tubercle Bacilli in Sputum. *Am J Respir Crit Care Med* 2010; **181**(2): 174-80.
6. Dhillon J, Fourie PB, Mitchison DA. Persister populations of *Mycobacterium tuberculosis* in sputum that grow in liquid but not on solid culture media. *J Antimicrob Chemother* 2014; **69**(2): 437-40.
7. Warner DF, Mizrahi V. Tuberculosis chemotherapy: the influence of bacillary stress and damage response pathways on drug efficacy. *Clin Microbiol Rev* 2006; **19**(3): 558-70.
8. Mitchison D, Davies G. The chemotherapy of tuberculosis: past, present and future. *Int J Tuberc Lung Dis* 2012; **16**(6): 724-32.
9. Wayne LG, Sohaskey CD. Nonreplicating persistence of *Mycobacterium tuberculosis*. *Annu Rev Microbiol* 2001; **55**: 139-63.
10. Esmail H, Barry CE, 3rd, Wilkinson RJ. Understanding latent tuberculosis: the key to improved diagnostic and novel treatment strategies. *Drug Discov Today* 2012; **17**(9-10): 514-21.
11. Davey HM, Kell DB. Flow cytometry and cell sorting of heterogeneous microbial populations: the importance of single-cell analyses. *Microbiol Rev* 1996; **60**(4): 641-96.
12. Muller S, Nebe-von-Caron G. Functional single-cell analyses: flow cytometry and cell sorting of microbial populations and communities. *FEMS Microbiol Rev* 2010; **34**(4): 554-87.
13. Akselband Y, Cabral C, Shapiro DS, McGrath P. Rapid mycobacteria drug susceptibility testing using Gel Microdrop (GMD) Growth Assay and flow cytometry. *J Microbiol Methods* 2005; **62**(2): 181-97.
14. DeCoster DJ, Vena RM, Callister SM, Schell RF. Susceptibility testing of *Mycobacterium tuberculosis*: comparison of the BACTEC TB-460 method and flow cytometric assay with the proportion method. *Clin Microbiol Infect* 2005; **11**(5): 372-8.
15. Fredricks BA, DeCoster DJ, Kim Y, Sparks N, Callister SM, Schell RF. Rapid pyrazinamide susceptibility testing of *Mycobacterium tuberculosis* by flow cytometry. *Journal of Microbiological Methods* 2006; **67**(2): 266-72.
16. Govender SdP, S.J.; van de Venter, M.; Hayes, C. Antibiotic susceptibility of multi-drug resistant *Mycobacterium tuberculosis* using flow cytometry. *Medical Technology SA* 2010; **24**(2): 25-8.
17. Reis RS, Neves I, Lourenco SLS, Fonseca LS, Lourenco MCS. Comparison of Flow Cytometric and Alamar Blue Tests with the Proportional Method for Testing Susceptibility of *Mycobacterium tuberculosis* to Rifampin and Isoniazid. *Journal of Clinical Microbiology* 2004; **42**(5): 2247-8.
18. Piuri M, Jacobs WR, Jr., Hatfull GF. Fluoromycobacteriophages for rapid, specific, and sensitive antibiotic susceptibility testing of *Mycobacterium tuberculosis*. *PLoS One* 2009; **4**(3): e4870.
19. Moore AV, Kirk SM, Callister SM, Mazurek GH, Schell RF. Safe determination of susceptibility of *Mycobacterium tuberculosis* to antimycobacterial agents by flow cytometry. *J Clin Microbiol* 1999; **37**(3): 479-83.

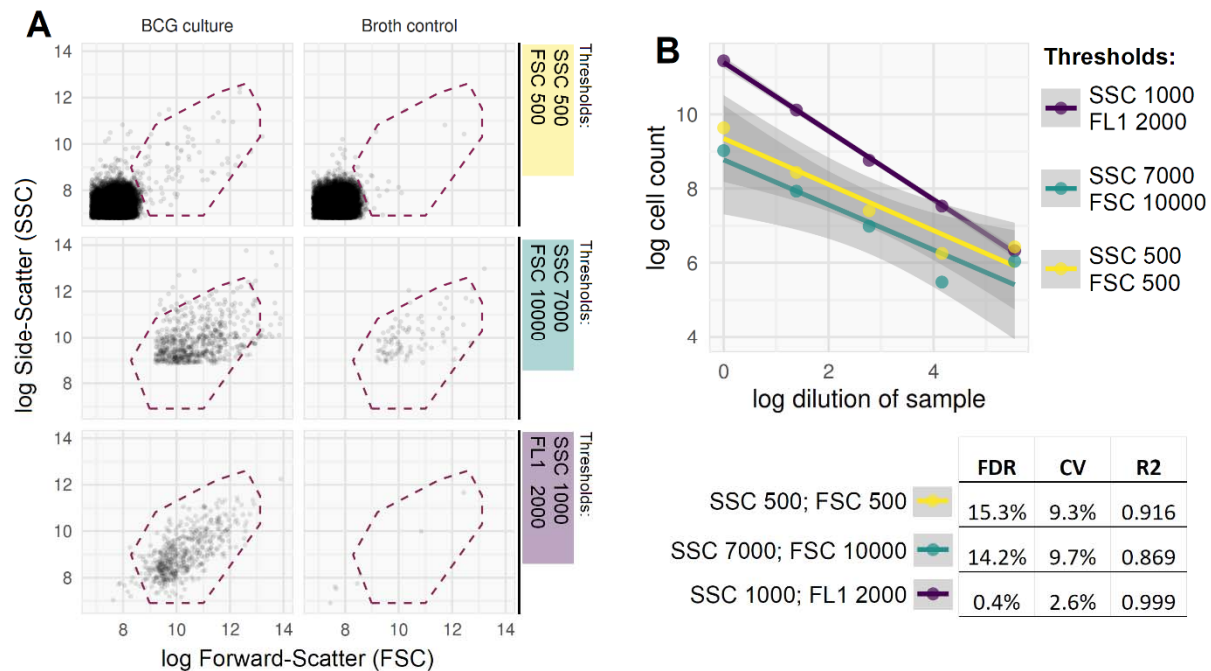
20. Bownds SE, Kurzynski TA, Norden MA, Dufek JL, Schell RF. Rapid susceptibility testing for nontuberculosis mycobacteria using flow cytometry. *J Clin Microbiol* 1996; **34**(6): 1386-90.
21. Norden MA, Kurzynski TA, Bownds SE, Callister SM, Schell RF. Rapid susceptibility testing of *Mycobacterium tuberculosis* (H37Ra) by flow cytometry. *J Clin Microbiol* 1995; **33**(5): 1231-7.
22. Vena RM, Munson EL, DeCoster DJ, et al. Flow cytometric testing of susceptibilities of *Mycobacterium avium* to amikacin, ciprofloxacin, clarithromycin and rifabutin in 24 hours. *Clin Microbiol Infect* 2000; **6**(7): 368-75.
23. Hammond RJ, Baron VO, Oravcova K, Lipworth S, Gillespie SH. Phenotypic resistance in mycobacteria: is it because I am old or fat that I resist you? *J Antimicrob Chemother* 2015; **70**(10): 2823-7.
24. Gonzalez YMJA, Zaragoza-Contreras R, Guadarrama-Medina R, et al. Evaluation of the cell growth of mycobacteria using *Mycobacterium smegmatis* mc2 155 as a representative species. *J Microbiol* 2012; **50**(3): 419-25.
25. Shi L, Gunther S, Hubschmann T, Wick LY, Harms H, Muller S. Limits of propidium iodide as a cell viability indicator for environmental bacteria. *Cytometry A* 2007; **71**(8): 592-8.
26. James BW, Williams A, Marsh PD. The physiology and pathogenicity of *Mycobacterium tuberculosis* grown under controlled conditions in a defined medium. *J Appl Microbiol* 2000; **88**(4): 669-77.
27. Resnick MS, S.; Bercovier, H. Bacterial membrane potential analysed by spectrofluorocytometry. *Current Microbiology* 1985; **12**: 183-6.
28. Ibrahim P, Whiteley AS, Barer MR. SYTO16 labelling and flow cytometry of *Mycobacterium avium*. *Lett Appl Microbiol* 1997; **25**(6): 437-41.
29. Yi WC, Hsiao S, Liu JH, et al. Use of fluorescein labelled antibody and fluorescence activated cell sorter for rapid identification of *Mycobacterium* species. *Biochem Biophys Res Commun* 1998; **250**(2): 403-8.
30. Qin D, He X, Wang K, Tan W. Using fluorescent nanoparticles and SYBR Green I based two-color flow cytometry to determine *Mycobacterium tuberculosis* avoiding false positives. *Biosens Bioelectron* 2008; **24**(4): 626-31.
31. Soejima T, Iida K, Qin T, Taniai H, Yoshida S. Discrimination of live, anti-tuberculosis agent-injured, and dead *Mycobacterium tuberculosis* using flow cytometry. *FEMS Microbiol Lett* 2009; **294**(1): 74-81.
32. Burdz TVN, Wolfe J, Kabani A. Evaluation of sputum decontamination methods for *Mycobacterium tuberculosis* using viable colony counts and flow cytometry. *Diagnostic Microbiology and Infectious Disease* 2003; **47**(3): 503-9.
33. Hendon-Dunn CL, Doris KS, Thomas SR, et al. A flow cytometry method for rapidly assessing *M. tuberculosis* responses to antibiotics with different modes of action. *Antimicrob Agents Chemother* 2016.
34. Shapiro HM. Flow cytometry of bacterial membrane potential and permeability. *Methods Mol Med* 2008; **142**: 175-86.
35. Ryan C, Nguyen BT, Sullivan SJ. Rapid assay for mycobacterial growth and antibiotic susceptibility using gel microdrop encapsulation. *J Clin Microbiol* 1995; **33**(7): 1720-6.
36. Scott LE, Gous N, Cunningham BE, et al. Dried culture spots for Xpert MTB/RIF external quality assessment: results of a phase 1 pilot study in South Africa. *J Clin Microbiol* 2011; **49**(12): 4356-60.
37. Kirk SM, Schell RF, Moore AV, Callister SM, Mazurek GH. Flow cytometric testing of susceptibilities of *Mycobacterium tuberculosis* isolates to ethambutol, isoniazid, and rifampin in 24 hours. *J Clin Microbiol* 1998; **36**(6): 1568-73.
38. Pina-Vaz C, Costa-Oliveira S, Rodrigues AG, Salvador A. Novel method using a laser scanning cytometer for detection of mycobacteria in clinical samples. *Journal of Clinical Microbiology* 2004; **42**(2): 906-8.
39. Tuma RS, Beaudet MP, Jin X, et al. Characterization of SYBR Gold nucleic acid gel stain: a dye optimized for use with 300-nm ultraviolet transilluminators. *Anal Biochem* 1999; **268**(2): 278-88.

40. Ryan GJ, Shapiro HM, Lenaerts AJ. Improving acid-fast fluorescent staining for the detection of mycobacteria using a new nucleic acid staining approach. *Tuberculosis (Edinb)* 2014; **94**(5): 511-8.
41. Weston SA, Parish CR. New fluorescent dyes for lymphocyte migration studies. Analysis by flow cytometry and fluorescence microscopy. *J Immunol Methods* 1990; **133**(1): 87-97.
42. Saito K, Warriar T, Somersan-Karakaya S, et al. Rifamycin action on RNA polymerase in antibiotic-tolerant *Mycobacterium tuberculosis* results in differentially detectable populations. *Proc Natl Acad Sci U S A* 2017; **114**(24): E4832-E40.
43. Davies GR. Early clinical development of anti-tuberculosis drugs: science, statistics and sterilizing activity. *Tuberculosis (Edinb)* 2010; **90**(3): 171-6.
44. Akerlund T, Nordstrom K, Bernander R. Analysis of cell size and DNA content in exponentially growing and stationary-phase batch cultures of *Escherichia coli*. *J Bacteriol* 1995; **177**(23): 6791-7.
45. Ferullo DJ, Cooper DL, Moore HR, Lovett ST. Cell cycle synchronization of *Escherichia coli* using the stringent response, with fluorescence labeling assays for DNA content and replication. *Methods* 2009; **48**(1): 8-13.
46. Barrett TC, Mok WWK, Murawski AM, Brynildsen MP. Enhanced antibiotic resistance development from fluoroquinolone persisters after a single exposure to antibiotic. *Nat Commun* 2019; **10**(1): 1177.
47. Bos J, Zhang Q, Vyawahare S, Rogers E, Rosenberg SM, Austin RH. Emergence of antibiotic resistance from multinucleated bacterial filaments. *Proc Natl Acad Sci U S A* 2015; **112**(1): 178-83.
48. Sun L, Alexander HK, Bogos B, Kiviet DJ, Ackermann M, Bonhoeffer S. Effective polyploidy causes phenotypic delay and influences bacterial evolvability. *PLoS Biol* 2018; **16**(2): e2004644.
49. Wayne LG. Synchronized replication of *Mycobacterium tuberculosis*. *Infect Immun* 1977; **17**(3): 528-30.
50. Ditse Z, Lamers MH, Warner DF. DNA Replication in *Mycobacterium tuberculosis*. *Microbiol Spectr* 2017; **5**(2).
51. Bull AT. The renaissance of continuous culture in the post-genomics age. *J Ind Microbiol Biotechnol* 2010; **37**(10): 993-1021.
52. Hoskisson PA, Hobbs G. Continuous culture--making a comeback? *Microbiology* 2005; **151**(Pt 10): 3153-9.
53. Carr EL, Eales K, Soddell J, Seviour RJ. Improved permeabilization protocols for fluorescence in situ hybridization (FISH) of mycolic-acid-containing bacteria found in foams. *J Microbiol Methods* 2005; **61**(1): 47-54.
54. Cimino M, Alamo L, Salazar L. Permeabilization of the mycobacterial envelope for protein cytolocalization studies by immunofluorescence microscopy. *BMC Microbiol* 2006; **6**: 35.
55. Evans JC, Trujillo C, Wang Z, et al. Validation of CoaBC as a bactericidal target in the coenzyme A pathway of *Mycobacterium tuberculosis*. *ACS Infect Dis* 2016; **2**(12): 958-68.
56. Manina G, McKinney JD. A single-cell perspective on non-growing but metabolically active (NGMA) bacteria. *Curr Top Microbiol Immunol* 2013; **374**: 135-61.
57. Caire-Brandli I, Papadopoulos A, Malaga W, et al. Reversible lipid accumulation and associated division arrest of *Mycobacterium avium* in lipoprotein-induced foamy macrophages may resemble key events during latency and reactivation of tuberculosis. *Infect Immun*. 2014; **82**(2):476-490.
58. Liu J, Gefen O, Ronin I, Bar-Meir M, Balaban NQ. Effect of tolerance on the evolution of antibiotic resistance under drug combinations. *Science*. 2020; **367**(6474):200-204.
59. McGrath M, Gey van Pittius NC, van Helden PD, Warren RM, Warner DF. Mutation rate and the emergence of drug resistance in *Mycobacterium tuberculosis*. *J Antimicrob Chemother*. 2014; **69**(2):292-302
60. Porter J, Deere D, Hardman M, Edwards C, Pickup R. Go with the flow – use of flow cytometry in environmental microbiology. *FEMS Microbiology Ecology* 1997; **24**(2): 93-101.

61. Wang Y, Hammes F, De Roy K, Verstraete W, Boon N. Past, present and future applications of flow cytometry in aquatic microbiology. *Trends Biotechnol* 2010; 28(8): 416-24.
62. Hassard FW, R. Understanding the Use of Flow Cytometry for Monitoring of Drinking Water.: Department for Environment, Food & Rural Affairs Drinking Water Inspectorate / Cranfield Water Science Institute, 2019.
63. Laplace-Builhe C, Hahne K, Hunger W, Tirilly Y, Drocourt JL. Application of flow cytometry to rapid microbial analysis in food and drinks industries. *Biol Cell* 1993; 78(1-2): 123-8.
64. Lin PL, Ford CB, Coleman MT, et al. Sterilization of granulomas is common in active and latent tuberculosis despite within-host variability in bacterial killing. *Nat Med*. 2014;20(1):75-79.1.
65. Hahne F, LeMeur N, Brinkman RR, et al. flowCore: a Bioconductor package for high throughput flow cytometry. *BMC Bioinformatics* 2009; 10: 106.
66. R Core Team (2013). R: A language and environment for statistical computing. R Foundation for Statistical Computing, Vienna, Austria. ISBN 3-900051-07-0, URL <http://www.R-project.org/>.
67. Charrad M, Ghazzali N, Boiteau V, Niknafs A. NbClust: An R Package for Determining the Relevant Number of Clusters in a Data Set. *2014*. 2014;61(6):36.
68. Benaglia T, Chauveau D, Hunter DR, Young D. mixtools: An R Package for Analyzing Finite Mixture Models. *Journal of Statistical Software*, 2009; 32(6), 1-29. <http://www.jstatsoft.org/v32/i06/>.
69. Bates D, Mächler M, Bolker B, Walker S. Fitting Linear Mixed-Effects Models Using lme4. *Journal of Statistical Software*, 2015; 67(1), 1–48. doi: [10.18637/jss.v067.i01](https://doi.org/10.18637/jss.v067.i01).
70. Johannes Schindelin, Ignacio Arganda-Carreras, Erwin Frise, et al. Fiji: an open source platform for biological image-analysis. *Nature Methods* 2012; 9(7): 676-682.



**Figure 1. Comparison of 3 thresholding strategies in heat killed and SYBR-gold stained mid-log phase BCG broth culture.**

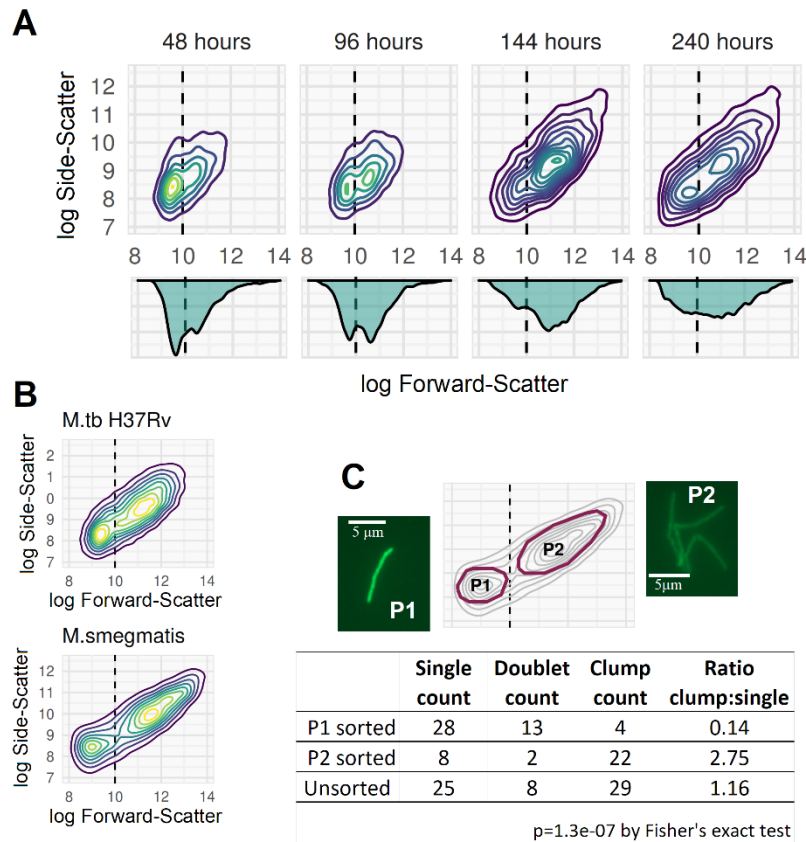


**A.** Example FCM plots for three thresholding strategies (rows 1-3) applied to *M. bovis* BCG broth culture (column 1) and cell-free broth (cell-free negative control, column 2). Counts are extracted for the gated population (events within dashed red line), which is placed to maximise the count in BCG broth and minimise the count in the cell-free control. Recorded events in the low light scatter value thresholding (first row) are dominated by debris/noise, seen as a dense population with low SSC and FSC values in lower left quadrant; this is equally apparent in the cell-free control. Higher light scatter thresholding (second row) excludes these events, but still records a substantial portion of higher SSC/FSC noise (seen in cell-free control), and the threshold level appears to bisect the ‘real’ cell population; *i.e.*, losing cells from analysis. By contrast, the thresholding based on fluorescence (third row) is qualitatively better, with very few false positive events in the cell-free control, and detection of a discrete cell population in BCG broth which is not artificially bisected.

**B.** Greater internal consistency in the FL1/SSC thresholding strategy, with less error across serial dilutions of a *M. bovis* BCG culture. Quantitative evidence of improved absolute count validity includes a lower false discovery rate (FDR, defined as false positive cell count in cell-free control divided by paired cell count from broth); lower coefficient of variation (CV, calculated by standard deviation/mean from 5 technical replicates, averaged for 3 biological replicates); and higher R<sup>2</sup> from linear fit across serial dilution series (one biological replicate as shown in figure;  $p < 0.001$  for F test comparing FL1/SSC to either FSC/SSC strategy; 95% confidence intervals for linear fit shown with grey shaded areas).



Figure 2. Identifying mycobacterial clumping with FCM.

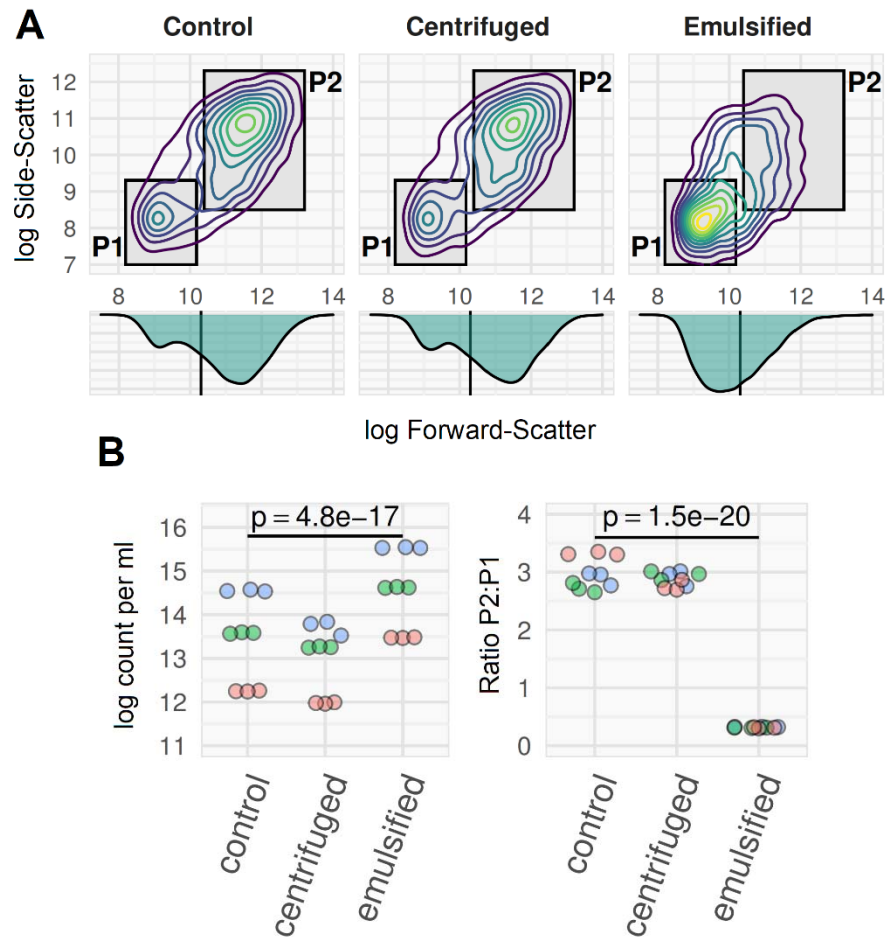


**A.** 2D-density plots of FSC v SSC on log scale for a culture of *M. bovis* BCG grown with 0.15% v/v Tween80 at 180 rpm. Plots are from samples taken at 48, 96, 144, and 240 hours after bacilli were sub-cultured from a log-phase starter culture into pre-warmed broth (early, early-mid, late-mid and late log-phase, respectively). Samples were diluted 10-fold or 100-fold (later samples) in 0.25% v/v Tween80 PBS and sonicated for 60 seconds prior to flow cytometry. The tail of higher SSC and FSC events at 48-hours is seen to develop into a discrete second subpopulation by 96-hours, which continues to expand into a higher SSC and FSC region and become the predominant subpopulation by the end of log-phase. All plots are constructed from 5000 events.

**B.** *M. tuberculosis* and *M. smegmatis* processed as above (both mid-late log phase) also develop dual populations separating on FSC and SSC, replicating the *M. bovis* BCG findings.

**C.** *M. smegmatis* sample was run on a BioRad S3 cell sorter with P1 and P2 sorted for downstream fluorescence microscopy (representative images shown). *M. smegmatis* was used for cell sorting owing to concerns about aerosolising *M. tuberculosis* or *M. bovis* BCG. P1 comprised majority single cells or doublets, while P2 comprised majority clumps (manually quantified from fluorescence microscopy images).

Figure 3. Needle-emulsification, but not vortex or sonication, disrupt clumps and increases cell counts

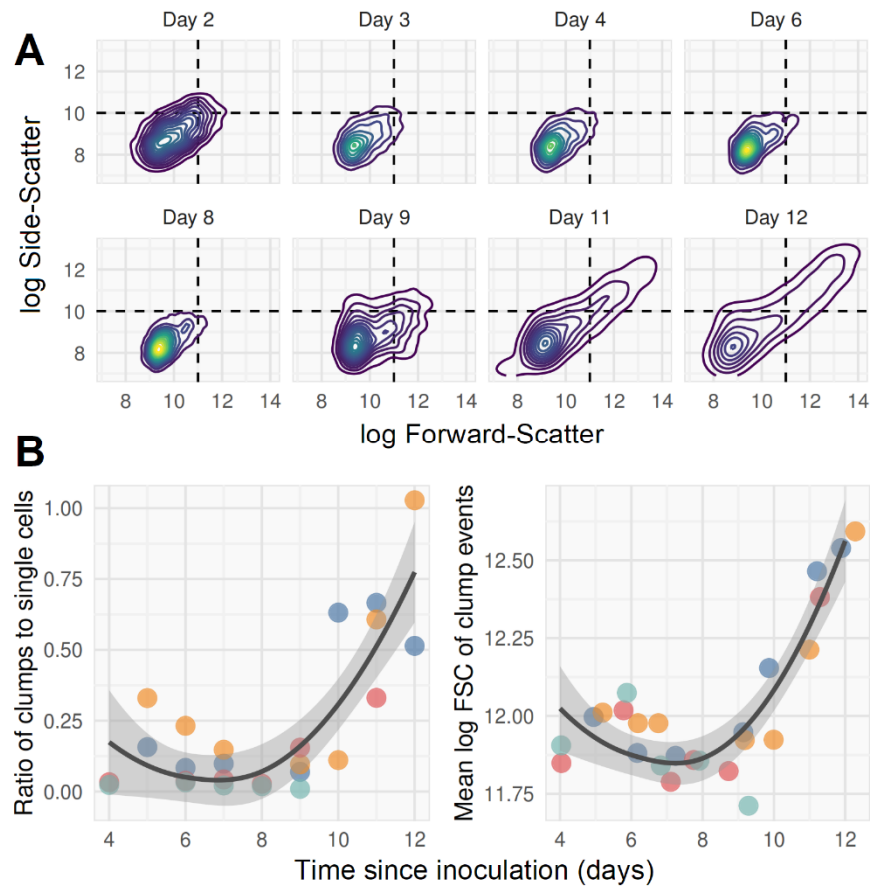


Mid-log phase culture of *M. smegmatis* grown in 0.15% v/v Tween80 7H9 with 150 rpm agitation and diluted 10-fold in 0.15% v/v Tween80 PBS and stained with Calcein-AM prior to FCM on a BD Accuri C6. Data acquisition with thresholds SSC>1000 and FL1>2000. Samples were processed by 60 second vortex, or by 60 second vortex followed by 5 minutes sonication in water bath, or by both these methods followed by needle emulsification (12 passes through a double Luer lock-ended, 25 Gauge, 4-inch, micro-emulsifying needle with a reinforcing bar (Cadence Inc.).

**A.** Two populations are seen which are differentiated by light-scatter: single cells (P1) and clumps (P2). Qualitatively, vortex and sonication processing did not disrupt P2 population (clumps), but needle emulsification (far right plot) shifted events from predominantly P2 (clumps) to predominantly P1 (single cells).

**B.** Counts of CFUs or FCM events with three-replicates from 3 independent cultures (purple, green, yellow dots). Emulsification resulted in a greater number of CFU and decreased the P2 count while increasing the P1 count substantially. The apparent total cell counts were increased by emulsification by an order of magnitude: both CFU count and total flow cytometry CA positive count increased by half to one unit on log scale. This can be interpreted as resulting from clumps (P2 population) being disaggregated into single cells (P1). The p-values were determined from repeated-measures ANOVA by cell-disruption method.

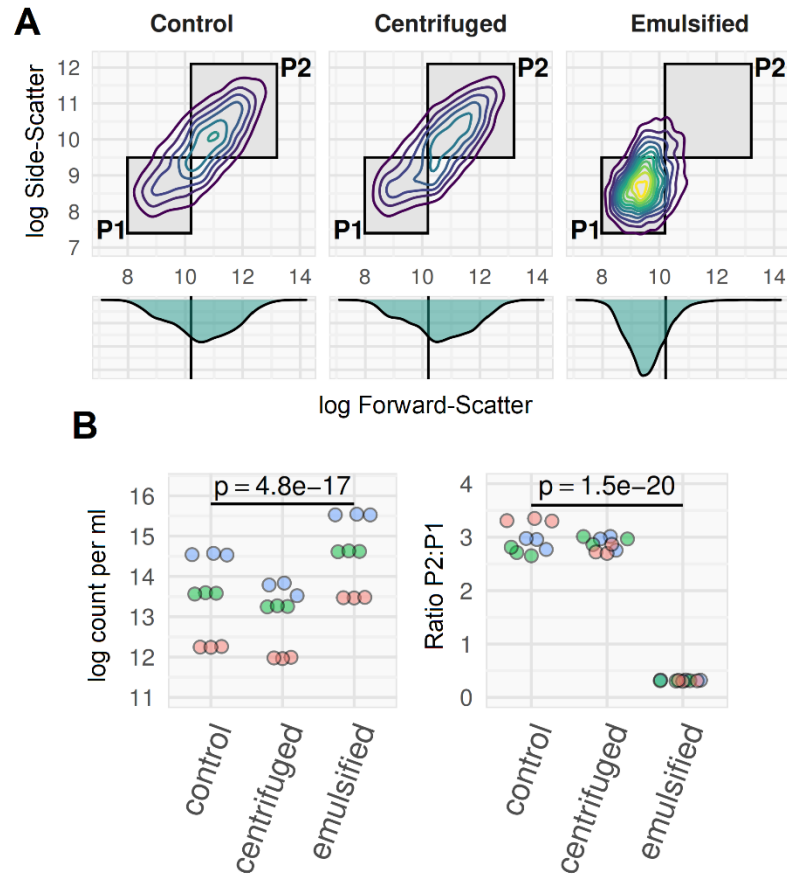
Figure 4. **Clumps which are resistant to disruption by emulsification eventually emerge in late log-phase cultures.**



**A.** *M. bovis* BCG culture in 0.15% v/v Tween80 7H9 with 150 rpm agitation and diluted 10-fold in 0.15% v/v Tween80 PBS before bacilli were heat-killed and stained with SYBR-gold. Samples were needle-emulsified (12 passes through a double Luer lock-ended, 25 Gauge, 4-inch, micro-emulsifying needle) prior to FCM on BD Accuri C6; data acquisition with thresholds SSC>1000 and FL1>1000. Timepoints are days post inoculation into pre-warmed broth from log phase starter culture. A long tail of clumps, extending into the upper-right quadrant of higher SSC and FSC, emerges from around day 9, at OD<sub>600</sub> ~ 0.3. Clumps were defined as events with SSC and FSC values greater than 10-log and 11-log (events in upper right quadrant of plots).

**B.** Clumps and single cells quantified by flow cytometry (four independent replicates of data represented by A; replicates are shown with different colours). Emulsification appears able to disrupt clumps until late log phase (~day 8), when both the ratio of clumps to single cells and size (approximated by mean FSC) of clumps rise rapidly. Line of best fit with 95% confidence interval band is a LOESS regression line ignoring dependence by replicate.

Figure 5. **Ratio of clumped to single-cell *M. smegmatis* is not altered by low-g centrifugation.**



Three mid-log phase *M. smegmatis* cultures grown in 0.05% Tween80 7H9 with continuous agitation at 150 rpm (3 biological replicates shown in blue, green and red), processed three ways. **Control sample:**  $10^{-1}$  dilution in 0.1% Tween80 PBS, no physical disruption. **Centrifuge sample:** 10ml + 5ml 0.1% Tween80 PBS; spun in 15ml centrifuge tubes at  $120 \times g$  for 8 minutes with no brake. **Emulsified sample:**  $10^{-1}$  dilution in 0.1% Tween80 PBS, 12x needle emulsified. Supernatant used for counts, as per ref 42 main manuscript. All samples heat-killed and stained with SYBR-gold prior to flow cytometry on BD Accuri-C6, with thresholding on SSC and FL1. Data are for three technical replicates of each culture.

**A.** Qualitatively, the FSC by SSC flow plots were similar for centrifuge method and control, compared to the needle-emulsified sample where the cell-clump population (P2) was not evident.

**B.** The ratio of clumps to single cells (p2:p1) was the same in the control and centrifuge preparations, but was much lower (and with less variation across replicates) with emulsification. Apparent cell counts were lower with centrifugation (owing to loss of cells in pellet) and higher with emulsification (owing to disruption of clumps). Three independent culture replicates (read, blue, and green; each processed 3 times in each condition for technical replicates); p-values from repeated measures ANOVA (technical replicates nested within culture replicates).

Figure 6. Schematic for final FCM count SOP used in *M. bovis* BCG culture growth & time-kill dynamics experiments

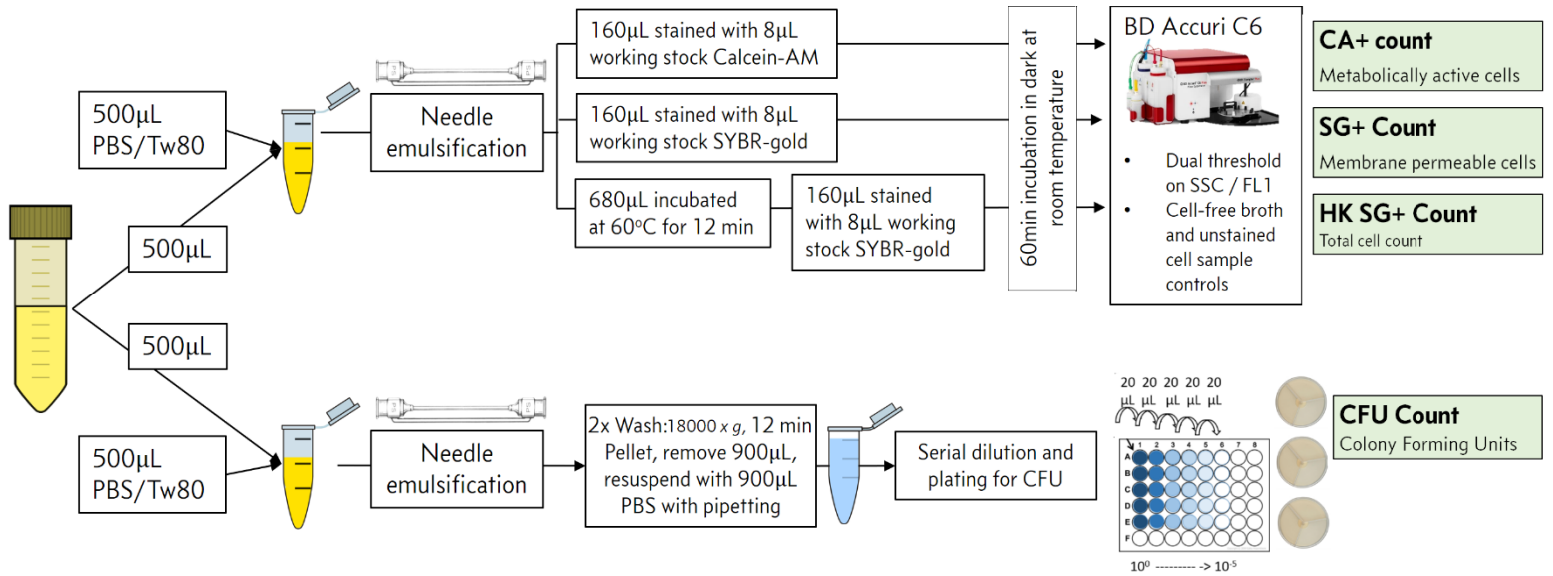
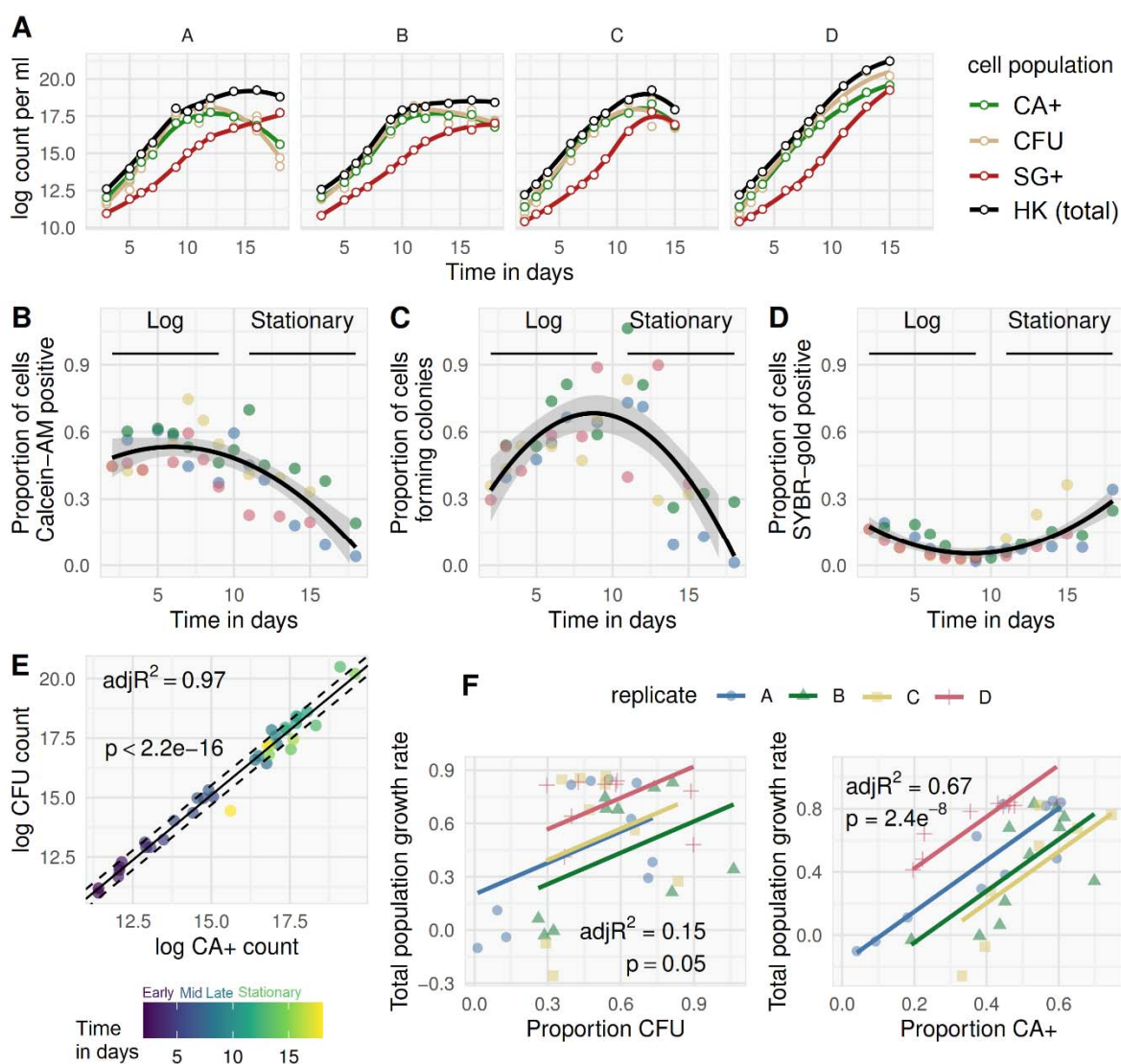


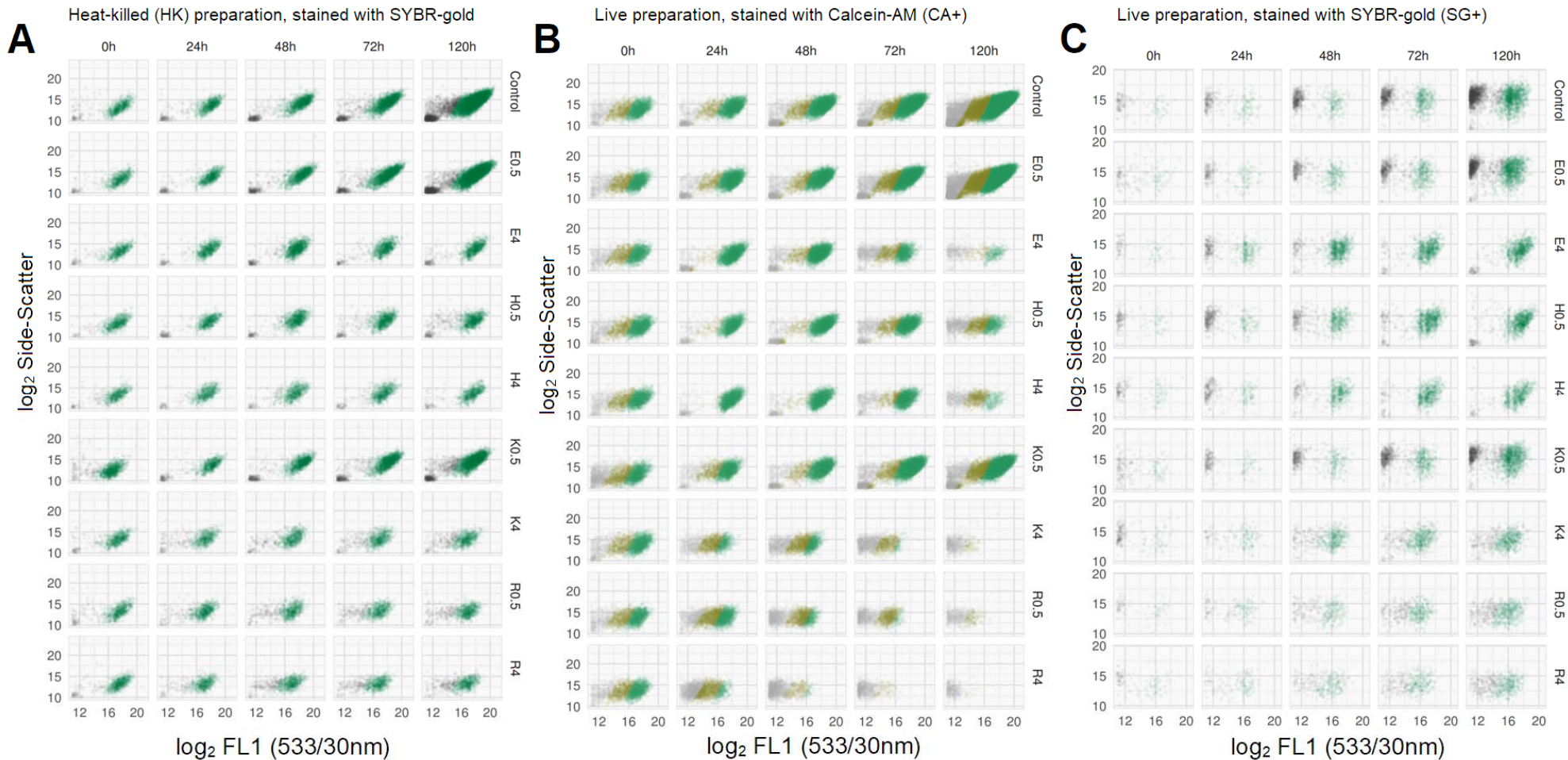
Figure 7. **Bacillary population dynamics during standard growth in culture**



Four independent *M. bovis* BCG cultures (replicates i to iv), grown in 50ml 0.15% v/v Tween80 7H9, 500ml tissueculture flasks at 150 rpm agitation, were serially quantified by CFU and FCM counts (method outlined in figure 6) between 2 and 15 days after inoculation into pre-warmed broth from a log phase starter culture. **(A)** Using the heat-killed SYBR-gold stained (HK) cell count as total cell denominator, the proportion of bacilli which were Calcein-AM positive (CA+), colony-forming (CFU), and permeable to SYBR-gold without heat-killing (SG+) are shown over time post inoculation **(B-D)**; each replicate is plotted using a different colour; LOESS line-of-best-fit and 95% CI shown for the observations aggregated across replicates. Linear correlation between log CA+ and log CFU counts was strong **(E)**, but with a dependency on phase of growth (time in days from inoculation shown by colour; non-constant variance (NCV) test for heteroscedasticity, p=0.03, dashed lines are +/- 1 SD of residual variation). Rate of population growth is defined as instantaneous rate of change in total cell count (slope of the tangent to the curve at a given timepoint; *i.e.*, first derivative of the growth curve). Rate of total population growth was regressed on proportion of bacilli able to form colonies, or on proportion CA+ **(F)**, at any given timepoint, with each replicate (i to iv, again shown by colour) allowed to differ by intercept but not slope.

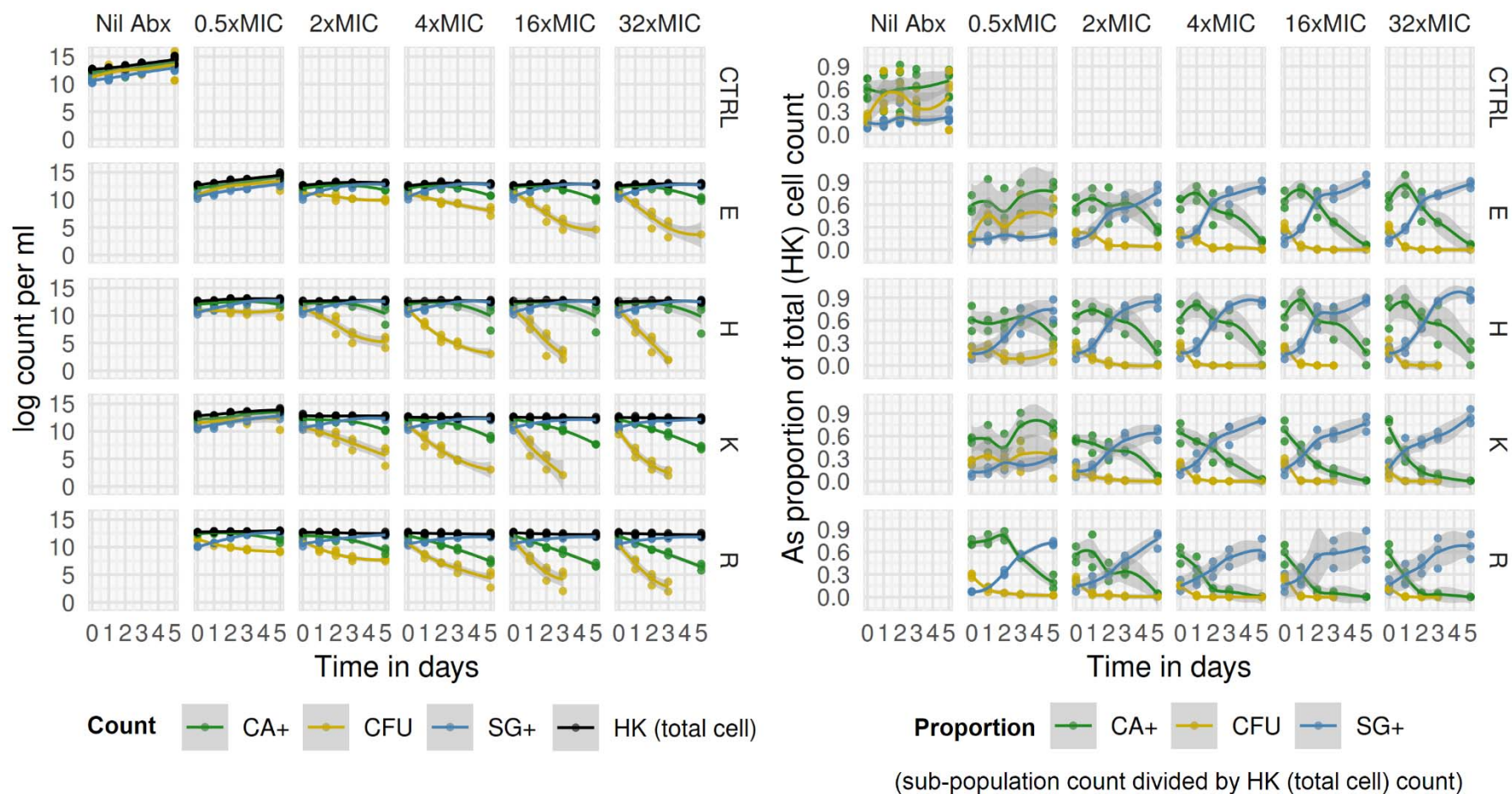


Figure 8. Raw FMC plots of HK, CA+, and SG+ events for selected antimicrobial conditions and timepoints.



Raw FMC data from one of three independent replicates. SYBR-gold stained heat-killed (HK) samples (A, left), Calcein-AM stained live samples (B, middle), and SYBR-gold stained live samples (C, right), by antimicrobial condition (rows) and time-point (hours) post introduction of antimicrobials (columns). Antimicrobial indicated by letter prefix (E, ethambutol; H, isoniazid; K, kanamycin; R, rifampicin) and concentration in multiples of MIC<sub>99</sub> by suffix letter (*e.g.*, R4 = rifampicin at 4x MIC). FCM events in each plot are coloured by K-means clustering on all light-scatter and fluorescence dimensions – an unsupervised classification (machine learning) algorithm used to define subpopulations without subjective manual placement of gates.

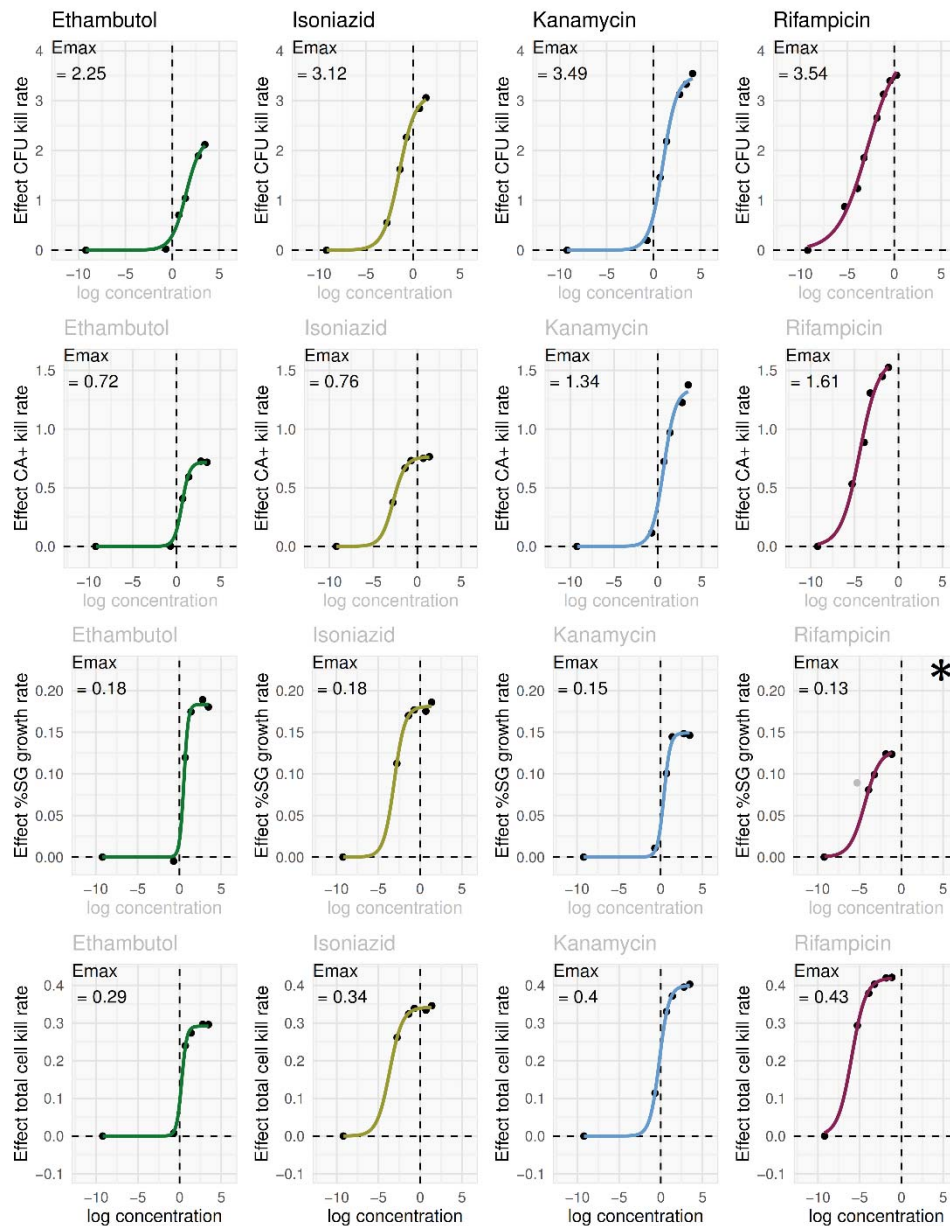
Figure 9. Time-kill curves generated through FCM defined cell populations and CFU counts



Data from three replicates. Counts (left panel) and proportions (right panel) by cell population [CA+ = Calcein-AM-stained in live samples; CFU = colony forming units; SG+ = SYBR-gold-stained in live samples; HK = SYBR-gold-stained in heat-killed samples] over time by antimicrobial condition. Antimicrobial indicated by letter in rows (E, ethambutol; H, isoniazid; K, kanamycin; R, rifampicin; CTRL, antimicrobial-free ["Nil Abx"] broth) and concentration in multiples of MIC in columns. Non-parametric Loess regression line and shaded 95% confidence intervals shown. Proportions are derived using HK count as a total cell count denominator (*i.e.* CA+/HK, SG+/HK, CFU/HK).



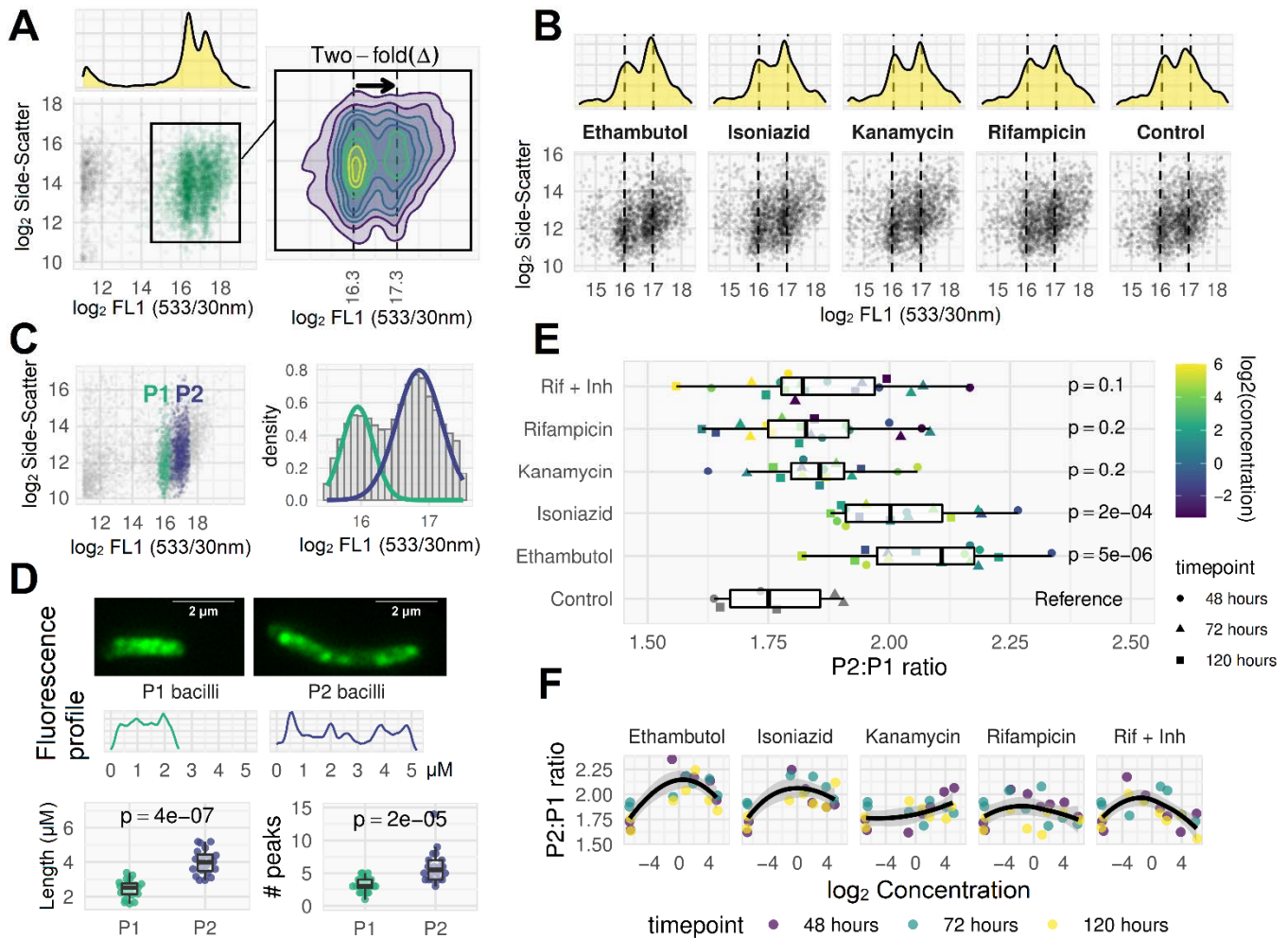
Figure 10.  $E_{max}$  models applied to time-kill data from FCM defined cell population and CFU counts



The time-kill data in figure 9 were modelled using a linear mixed-effects model to extract an estimate of mono-exponential elimination rate for each antimicrobial condition as a summary pharmacodynamic (PD) measure for each FCM defined cell population and CFU counts. Antimicrobial effects extracted from these models were related to drug concentration for each antimicrobial using a standard sigmoidal  $E_{max}$  PK/PD model, shown here for each antimicrobial (columns) and each cell population (rows).

\* A sigmoidal  $E_{max}$  model could not be fit for rifampicin %SG+ growth rate data due to non-convergence; the fit shown is from a model excluding the outlier data point at concentration 0.005 mg/ml (-5.3 on log scale). When this data point (indicated in grey) was excluded, the model converged.

Figure 11. **Distinct pharmacodynamics of SYBR-gold-positive sub-populations**



**A.** FCM plot for ethambutol-treated (4x MIC, 48 hours), SYBR-gold stained live bacilli. Two discrete sub-populations are visible, separated by approximately two-fold difference in fluorescence. These sub-populations were visible in most ethambutol- or isoniazid-treated cultures, but not readily visible in rifampicin or kanamycin FCM plots (figure 8). **B.** After membrane permeabilization at room temperature, these distinct sub-populations are visible under all conditions including the antimicrobial-free control. **C.** Clustering algorithm (Gaussian mixture model) used to label bacilli as P1 (lower SG fluorescence) or P2 (higher SG fluorescence). **D.** P1 and P2 bacilli sorted for downstream microscopy show different morphologies. A random selection of bacilli images from sorted P1 and P2 sub-populations were measured along their longitudinal axis using ImageJ to assess length and fluorescence profile (two examples shown). P2 bacilli were longer than P1 bacilli (mean 4.0 $\mu$ m versus 2.5 $\mu$ m) and contained approximately double the number of fluorescent 'peaks' (mean 6.1 versus 3.2; peaks defined by local maxima in a LOESS smoothing function applied to the fluorescence profile plots). **E.** The ratio of P2:P1 bacillary counts was dependent on antimicrobial: isoniazid and ethambutol exposure caused a relative rise in P2 bacilli compared to control, but the same effect was not seen for rifampicin or kanamycin. For the rifampicin plus isoniazid (Rif + Inh) combination treatment, the P2:P1 ratio matched the ratio obtained for rifampicin monotherapy, rather than isoniazid. All p-values were determined from a linear regression of P2:P1 ratio on antimicrobial category, with the antimicrobial-free control as reference category. **F.** Non-parametric Loess regression fitting P2:P1 ratio to log<sub>2</sub> concentration (black line with shaded 95% confidence interval) for each antimicrobial condition suggests the pharmacodynamic effect may be non-linearly dependent on concentration.